Changes in the magnetotail configuration before near-Earth reconnection

K. Snekvik,[1] E. Tanskanen,[1,2] N. Østgaard,[2] L. Juusola,[1,2] K. Laundal,[3] E. I. Gordeev,[4] and A. L. Borg[5]

Received 29 July 2011; revised 29 November 2011; accepted 4 December 2011; published 28 February 2012.

[1] We have examined three typical substorm growth phase signatures in the magnetotail two hours before near Earth reconnection; namely current sheet thinning, field line stretching and increase in the lobe magnetic pressure. The reconnection events were identified from in situ measurements in the plasma sheet by the Cluster spacecraft. The events were signified by high speed plasma flows, often lasting more than one hour. The list of events contains time intervals with high solar wind driving and strong intensification in the auroral westward electrojet, and other intervals with weak driving and no intensification in the electrojet. Irrespective of the amount of driving, there was usually a significant thinning of the current sheet prior to the reconnection onsets. Multispacecraft measurements of the magnetic field revealed that the average thinning was from 24000 to 12000 km, lasting about an hour. In those events without thinning, the current sheet was thin for an extended period before reconnection. Furthermore, the thinning happens even when there is no increase in the lobe magnetic pressure in the same time interval. The magnetotail is often stretched for a long time before reconnection onset, and reconnection seems to commence only when the current sheet is thin enough. In those events with large increase in the lobe magnetic pressure before onset, there is also significant field line stretching.

Citation: Snekvik, K., E. Tanskanen, N. Østgaard, L. Juusola, K. Laundal, E. I. Gordeev, and A. L. Borg (2012), Changes in the magnetotail configuration before near-Earth reconnection, *J. Geophys. Res.*, *117*, A02219, doi:10.1029/2011JA017040.

1. Introduction

[2] The amount of magnetic flux in the magnetotail depends on the opening of magnetic flux on the dayside, and closing of magnetic flux on the nightside by magnetic reconnection. The angle at which the tail magnetopause flares and hence the angle of attack of the solar wind on it, is a balance between the solar wind ram pressure and the internal lobe magnetic pressure. Particle pressure can usually be ignored in the lobes, and the dynamic pressure dominates in the solar wind. More flux in the lobes may cause this flaring angle to increase, as does the push from the solar wind. This is consistent with an enhanced lobe magnetic pressure [e.g., *Fairfield*, 1985]. If the solar wind dynamic pressure varies in the same time, the relation between the lobe magnetic flux and pressure becomes more complicated. In a statistical study, *Caan et al.* [1975] found that the lobe magnetic field magnitude increases before the onset of midlatitude bays, and decreases afterwards. Hence, the lobe magnetic pressure enhancements are often considered an important substorm growth phase signature.

[3] Lobe pressure enhancement leads to a reconfiguration of the magnetic field lines in the plasma sheet. An example of this reconfiguration during a substorm growth phase was given by *Pulkkinen et al.* [1991]. They constructed a model of the near-Earth current systems to describe the observed development of the tail magnetic field. Increased lobe magnetic field strength was equivalent to an enhanced cross tail current in their model. This results in stretching of the magnetic field lines earthward of the enhanced current and more dipolar field tailward of it. A spacecraft in the plasma sheet can measure the stretching as a decrease in the magnetic field component normal to the current sheet, B_Z, which reflects the amount of current tailward and earthward of the spacecraft. *Pulkkinen et al.* [1991] found that current sheet thinning also occurred in the same time interval as lobe pressure enhancement and magnetic field line stretching, resulting in a decrease in the current sheet thickness of 90%. Statistically, current sheet thinning is observed to start 30–60 min before substorm onset identified from various observations such as geosynchronous injections, the auroral electrojet index, midtail

[1]Finnish Meteorological Institute, Helsinki, Finland.
[2]Department of Physics and Technology, University of Bergen, Bergen, Norway.
[3]Teknova AS, Kristiansand, Norway.
[4]Department of Physics of Earth, Saint Petersburg State University, St. Petersburg, Russia.
[5]European Space Research and Technology Center, European Space Agency, Noordwijk, Netherlands.

0148-0227/12/2011JA017040

dipolarizations and Pi2 pulsations; and to continue 10 min afterwards, when current sheet expansion starts [*Baumjohann et al.*, 1992; *Thompson et al.*, 2005].

[4] The decrease in the lobe magnetic pressure after substorm onset, corresponds to enhanced magnetotail reconnection. The observed timing of substorm signatures in the magnetotail will depend on the spacecraft location relative to the X-line. For X_{GSM} between -11 and -16 R_E, *Baumjohann et al.* [2000] found earthward flows and dipolarization to coincide with substorm onset. Simultaneously, tailward flows were observed beyond $X_{GSM} = -21$ R_E. Earthward flow and dipolarization were progressively observed further and further tailward, and about 45 min after onset they were observed tailward of 26 R_E. Their interpretation was that a near Earth neutral line (NENL) formed around 21 R_E, which in turn resulted in a dipolarization front at about 13 R_E. The dipolarization front moved tailward with about 50 km/s. When it reached the NENL, both were swept tailward. Consistent with this, *Hones* [1984] found that current sheet expansion occurs longer after substorm onset (defined from the AL-index) tailward of 17 R_E, compared to around 13 R_E.

[5] It has been suggested that thinning during substorm growth phase is a direct consequence of increased pressure from the lobes which compresses the current sheet [e.g., *Baumjohann et al.*, 1992; *Baker et al.*, 1996]. *Dmitrieva et al.* [2004] studied the lobe magnetic pressure during substorms. They found that thinning and stretching seem to occur independently of lobe pressure enhancements before onset. *Thompson et al.* [2005] found no average increase in the lobe pressure before earthward flow and dipolarization in the plasma sheet during substorms; although there was a current sheet thinning of 20 % .

[6] Although the energy release during substorms increases with the amount of flux in the tail at substorm onset [*Shukhtina et al.*, 2005; *Milan et al.*, 2009], it has not been possible to find a critical magnitude of the tail flux whichleads to reconnection [*Milan et al.*, 2007]. In case of a thick dipolar current sheet, as is usually the case in the magnetotail, thinning and stretching is needed in order for reconnection to occur. *Milan* [2009] has proposed that an enhanced positive B_Z makes the tail more resistant to reconnection.

[7] In this paper, three typical substorm growth phase signatures and their time development two hours before reconnection onset, are studied. They are lobe magnetic pressure enhancement, current sheet thinning and magnetic field line stretching. By taking advantage of four-points simultaneous measurements in space from Cluster, we are able to follow the time development of the current sheet thickness. This and other methods will be elaborated in the next section.

[8] To our knowledge, it is the first time these growth phase signatures have been studied in relation to reconnection events which have been identified solely from in situ measurements in the plasma sheet, and independently from substorm ground signatures. Thirteen reconnection events were identified and analyzed by *Borg et al.* [2007] and *Østgaard et al.* [2009]. Their selection criteria will only be summarized here. For each event the satellites had to observe: (1) A flow reversal in the X-direction; (2) a simultaneous B_Z-reversal; and (3) the quadrupolar magnetic signature due to the Hall current system in the reconnection region [*Sonnerup*, 1979].

2. Data Analysis

2.1. Data Products

2.1.1. Solar Wind Data

[9] The solar wind driving was quantified in terms of the effective dayside reconnection electric field [*Kan and Lee*, 1979]. It is calculated from solar wind magnetic field and velocity data (GSM):

$$E_D = V_X B_{YZ} \sin^2 \frac{\theta}{2}, \quad \tan\theta = \frac{|B_Y|}{B_Z}, \quad 0 \le \theta < \pi \tag{1}$$

This formula was recently used by *Milan et al.* [2008] to estimate the flux transport rate into the polar cap.

[10] Solar wind data was taken from the NASA/GSFC's High Resolution OMNI data set through OMNIWeb [*King and Papitashvili*, 2005]. (See also the OMNIWeb Internet page for more updated documentation.) Data which are time shifted to the Earth's bow shock, are available from four spacecraft, namely Geotail, Wind, ACE and IMP 8. The time shifts are not without uncertainties. The time shifted samples will arrive in a different sequence to the Earth than when they were observed. Three parameters exist in the OMNI data set to describe the uncertainty in the time shift. In this paper the standard deviation of the time shifts, in one minute time intervals, was used to evaluate the uncertainty. This parameter is called the RMS in the OMNI data set. In time intervals when data sets were available from more than one spacecraft in the solar wind, the data sets with lowest RMS were chosen.

2.1.2. Magnetotail Data

[11] The four identical spacecraft (C1, C2, C3 and C4) of the Cluster mission, are used for the magnetotail observations. Figure 1 shows their positions as tetrahedrons with one spacecraft in each vertex, in the YZ_{GSM} plane, as seen from the Earth. In event number 12 the tetrahedron is so small that it is not visible in Figure 1. The measurements are taken from the fluxgate magnetometer experiment (FGM) [*Balogh et al.*, 2001] and the Cluster Ion Spectrometry (CIS) [*Rème et al.*, 2001]. CIS consists of two detectors, namely the Hot Ion Analyzer (HIA), and the time-of-flight ion Composition Distribution Function (CODIF). The plasma measurements used here are derived from proton data from CODIF at C1 and C4 and ion data from HIA at C3.

2.2. Lobe Pressure and Magnetic Field

[12] Since the plasma pressure in the lobe usually is less than 0.01 nPa and therefore negligible compared to the magnetic pressure [*Angelopoulos et al.*, 1994], the relation between the total lobe pressure, P, and magnetic field B_L, is well approximated as $B_L = \sqrt{2\mu_0 P}$.

[13] The total pressure in the plasma sheet, is the sum of the thermal and magnetic pressures. According to the "tail approximation" described by *Birn* [1987], the total pressure is constant in the Z-direction. This has also been verified experimentally by *Baumjohann et al.* [1990] and *Nakamura et al.* [1999]. In the derivation it was assumed that B_Z is negligible compared to the other magnetic field components. In some of our events this was not the case. But if the other

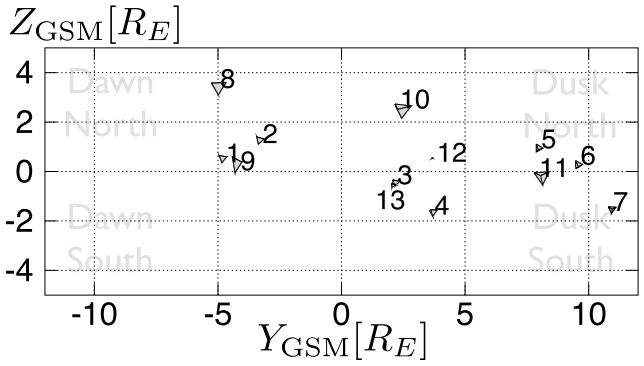

Figure 1. The Cluster positions in the YZ_{GSM} plane. The numbers 1–13 refer to the different events. In all events Cluster was near apogee at 19.6 R_E from the Earth. The size and shape of the Cluster configurations are indicated by tetrahedrons.

assumptions in the "tail approximation" are reasonable and B_Z is small in the lobes, it can be shown that the lobe pressure can be estimated as $P = p + B_{XY}^2/(2\mu_0)$, where p is the plasma pressure, and B_{XY} is the magnetic pressure due to the XY-components of the magnetic field.

[14] *Baumjohann et al.* [1988, 1989] found that the electron temperature is about 14% of the ion temperature in the plasma sheet. It follows that the lobe pressure is approximately $P = 1.14nkT + B_{XY}^2/(2\mu_0)$, where n and T are the ion density and temperature.

2.3. Coordinate System

[15] For the analysis below, it is important to use a coordinate system which reflects the orientation of the current sheet. Close to midnight the main component of the magnetic field is approximately along X_{GSM}, but as the distance from midnight increases, it will get an increasing component along Y_{GSM} due to the flaring of the magnetotail [*Kaymaz et al.*, 1994]. To account for this, a variance analysis is performed on the magnetic field during the satellite crossing of the plasma sheet, for each event. This can be done since Cluster has a polar orbit and thus stays at approximately the same local time in the plasma sheet during each orbit. Each crossing was identified from B_X and plasma β and lasted 2–12 hours. The direction with maximum variance $\mathbf{l}$, is taken as the X-direction. *Khrabrov and Sonnerup* [1998] showed that this is a good approximation for a current sheet where the current is unidirectional. The modified Y-direction is parallel with $\mathbf{Z}_{\mathrm{GSM}} \times \mathbf{l}$.

2.4. Harris Current Sheet Fitting

[16] The Cluster tetrahedron gives the possibility to separate between spatial and temporal variations in the plasma sheet. Many previous studies have attributed an increase of $|B_X|$, or other similar parameters, to current sheet thinning, in lack of more precise knowledge. Based on multispacecraft methods, the current sheet half thickness L, can be estimated by fitting measurements of the magnetic field component B_X, and the Cluster vertical positions Z_C, to an appropriate current sheet model, as demonstrated by *Nakamura et al.* [2002a].

[17] The most commonly used current sheet model was derived by *Harris* [1962]. This model was derived under several assumptions which may not be fulfilled in the plasma sheet. The structure of the cross tail current sheet have been observed to exhibit large variations from event to event [*Asano et al.*, 2005; *Runov et al.*, 2006]. In some cases, the current sheet is bifurcated, i.e., the current has one peak above and another below the neutral sheet. In other cases, it has an intense maximum near the neutral sheet. These distributions come in addition to the large time variability caused by numerous transient processes in the plasma sheet (see *Sharma et al.* [2008] for a review).

[18] For easier comparison with previous work, and because of no obviously better alternative, we use the Harris current sheet model in this paper as well. In the appendix, we investigate the effect different current sheet models has on the inferred current sheet thickness. It is found that the estimates are quite sensible to the current sheet model, but the time evolution is usually the same for different models. Thus, we believe we can use this technique to identify current sheet thinning.

[19] The most common way to write the Harris current sheet equation is $B_X/B_L = \tanh((Z - Z_0)/L)$ where Z_0 is the center of the current sheet. The equation is more useful for us in its inverted form:

$$Z = LZ_n + Z_0, \quad Z_n = \tanh^{-1}\frac{B_X}{B_L}. \tag{2}$$

[20] However, Z_0 was not of interest in this study and can be removed by subtracting the equation for one of the spacecraft, in this case Cluster 1, from the others. This gives $\Delta Z_i = L\Delta Z_{ni}$, where $\Delta Z_{ni} = Z_{ni} - Z_{n1}$. Finally, the real positions, Z_C, of Cluster are compared with those estimated above, and the current sheet thickness is found by minimizing

$$\sum_{i=2}^{4} (\Delta Z_{Ci} - L\Delta Z_{ni})^2, \quad i = 2 - 4 \tag{3}$$

with respect to L. The numbers refer to Cluster 1–4, and Cluster 1 is used as the reference spacecraft. When this fitting was done for high resolution magnetic field data, it was found that L exhibited large fluctuations with periods ranging from tens of seconds to a few minutes. Such fluctuations could be the result of applying a wrong model, or because of other sources of magnetic variation. Ten minutes median values for ΔZ_{ni} was the lowest time resolution which gave satisfactory results. However, most of the analysis in this paper is done for 30 min median values. We found that it was often better to calculate the median rather than the mean value, because a few large values often got a disproportional weight in the mean value.

[21] To further ensure the quality of the calculation, estimates which fulfilled one or more of the following criteria, were rejected.

1. The root mean square error of the least square fit was larger than 50 % of the separation between the spacecraft. This is the most straightforward indication that a wrong model has been used for the measurements.

2. The thickness is negative, or more than 20 times the Cluster separation. The first case is evidently not physical. In the latter case, the estimate becomes uncertain because the Cluster tetrahedron only covers a very small part of the current sheet.

3. The average Cluster position in the current sheet is more than one half thickness from the center. This is where $(Z - Z_0)/L > 1$, or equivalently where $B_X > .76B_L$.

[22] Figure 2 shows an example of a current sheet fitting. The left panel shows the least square fit for equation (3). The straight line is the best linear fit. It passes through zero, since there is no constant term in equation (3). The right panel shows a reconstructed current sheet based on this fit, and the approximate position of Cluster. The current sheet half thickness L, is shown with horizontal lines.

3. Results

3.1. Two Reconnection Events

[23] Figure 3 shows two examples of the reconnection events. The first is from 21 Aug 2002, and the second is three days earlier. In the top panel are the earthward and tailward flows, V_X. In the three next panels, are the three main parameters we will focus on in this paper; namely the normal component of the magnetic field, B_Z; the estimated lobe magnetic field, B_L; and the estimated current sheet half thickness, L. To better see the gradual time development of B_Z, B_L and L, 30 min median values are superposed on the higher resolution data. The effective dayside reconnection electric field, E_D, is shown in the bottom panel. The colored horizontal lines in the top panel mark when the satellites are within 1 L from the center of the current sheet.

[24] The red vertical lines in the center, mark the reconnection onsets. In these two events, it is quite easy to identify the onsets from the tailward flow, $V_X < 0$. After onset there are reversals in both V_X and B_Z as expected when crossing the reconnection region.

[25] We will now focus on the two hours preceding reconnection onset. The two events occurred during very different solar wind conditions. In the first event, the average E_D before reconnection onset, is about 3.2 mV/m, while it is a magnitude smaller in the second event. In the 21 August event, B_Z and L decrease by about 8 nT and 11000 km, respectively. This is interpreted to be due to stretching of the tail magnetic field and current sheet thinning, respectively. Simultaneously, there is a substantial increase in the lobe magnetic field strength of about 15 nT or 60 %. Thus, this event shows the classic signatures of a substorm growth phase, where increase in the lobe pressure happens simul-

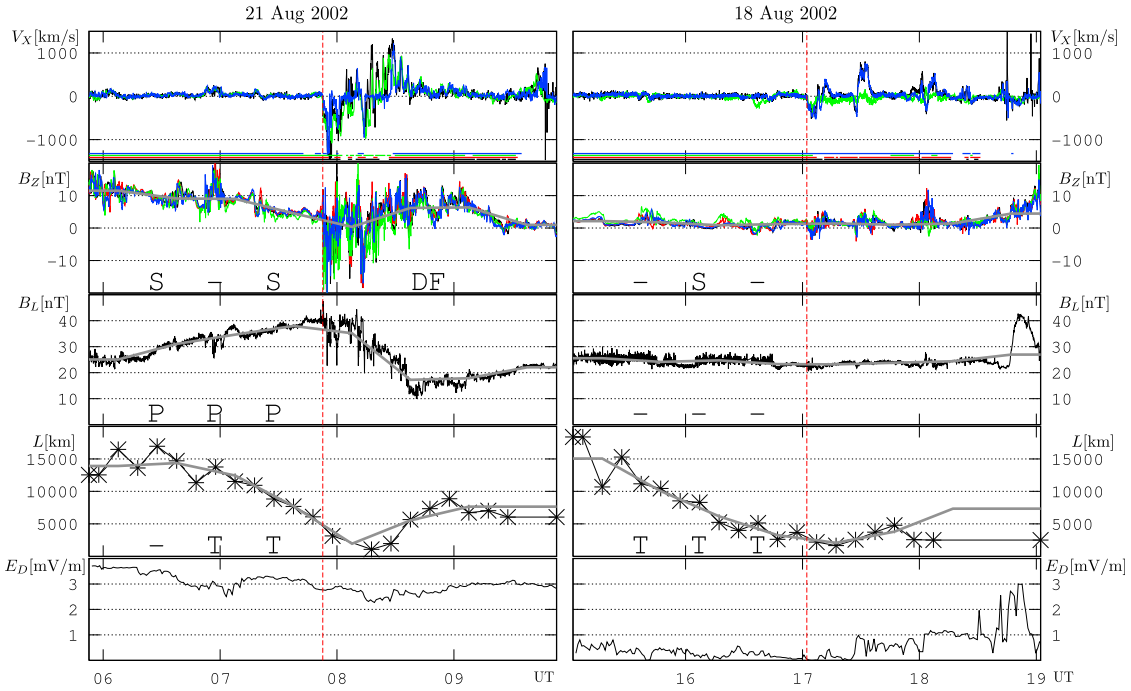

Figure 3. Measurements and estimated parameters from Cluster 1 (black), 2 (red), 3 (green), and 4 (blue). Figure 3 shows from top to bottom: The earthward and tailward flow, V_X; the northward and southward component of the magnetic field, B_Z; the estimated lobe magnetic field, B_L; the estimated current sheet half thickness, L; and the effective dayside reconnection electric field, E_D. The horizontal lines in the first panel mark when the space craft are within 1 L from the neutral sheet. The red line marks the start of the reconnection events as identified as the start of the tailward flow. Magnetic field line stretching, lobe pressure enhancement, current sheet thinning and dipolarization are denoted by S, P T and DF, respectively. Modified GSM coordinates are used.

from the current sheet center. Only those intervals which contained at least one sample with $|V_X| > 200$ km/s as well as flux transport $V_X B_Z - V_Z B_X > 10$ kWb/(R_Es), were kept. The second criterion was used to avoid purely field aligned flow. Finally, flow intervals separated by less than 30 min, were merged to calculate the durations in Table 1. A data gap at the end of the first event made it impossible to determine its duration.

[29] The start of the flow intervals will be referred to as *reconnection onset* throughout the text. It should be emphasized that these times are based on local measurements, and it is difficult to say if there is reconnection somewhere else in the magnetotail. It is also possible that reconnection has been going on for a while, when the Cluster spacecraft first see the flow, since the reconnection region may move.

[30] The earthward and tailward flow intervals are summarized in Figure 4. All times shown are relative to reconnection onset for each event. Red color indicates earthward flow, while blue color indicates tailward flow. Most events start with tailward flow, and all events end with earthward flow. Magnetic field line stretching, lobe pressure enhancement, current sheet thinning and dipolarization are identified as described in the previous subsection. A question mark means that a parameter was not available for that time interval.

[31] It can be seen that pressure enhancements (P) usually occur together with stretching (S), while both stretching and thinning (T) often occur alone. Another prominent feature is that reconnection onset usually occur after a period of either thinning or stretching, even in those cases where there are no pressure enhancements. This will be discussed in more detail in the next subsection.

[32] In order to put the reconnection events into a global context, some other measurements are included. The auroral images used by *Østgaard et al.* [2009] have been utilized to identify substorm onsets and local intensifications. These are shown with stars and crosses, respectively. In addition, the

Table 1. Nr–The Event Numbers, the Date and Time for the Onset of Each Event, and the Duration of the Flows Associated With Each Reconnection Event

Nr	Date and Time	Duration (min)
1	17 Aug 2001 16:23	–
2	22 Aug 2001 09:23	84
3	10 Sep 2001 07:48	10
4	15 Sep 2001 03:41	95
5	01 Oct 2001 09:26	47
6	08 Oct 2001 12:29	108
7	11 Oct 2001 03:25	109
8	18 Aug 2002 17:03	69
9	21 Aug 2002 07:54	74
10	13 Sep 2002 18:08	69
11	02 Oct 2002 21:20	72
12	19 Sep 2003 23:21	80
13	14 Sep 2004 22:44	45

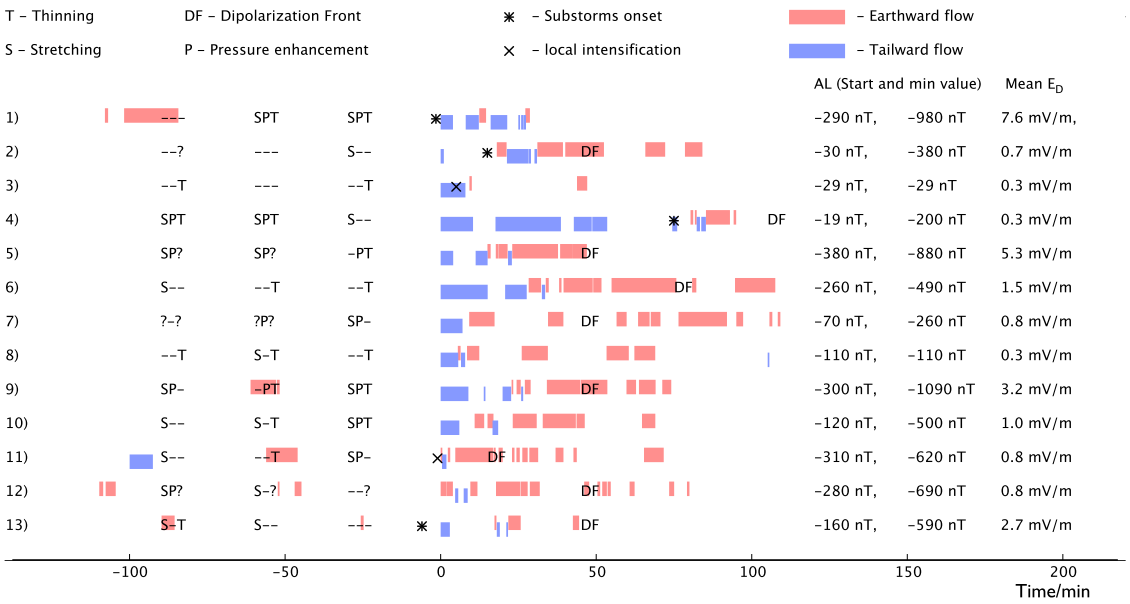

Figure 4. A summary of some key parameters from the reconnection events. All events are centered at reconnection onset. The letters mark current sheet thinning (T), magnetotail stretching (S), lobe pressure enhancement (P) and the dipolarization fronts (DF). Substorm onset and local intensifications are shown for the events where auroral images were available. The values of the AL index are shown at the start of each reconnection events, and when it has its lowest values. The mean effective dayside reconnection electric field, E_D, is calculated two hours before reconnection onset.

AL-index at the start of the reconnection events, and the minimum values during the reconnection events are included. It can be seen that the auroral westward electrojet usually is quite strong, and that it increases during the events. For comparison, *Tanskanen et al.* [2005] required a substorm onset to be followed by a decrease of the auroral electrojet index by at least 80 nT. Because of the coarse distribution of the AE magnetometers, it does not make any sense to determine the precise times of the onsets of the magnetic intensifications. The rightmost column shows the average effective dayside reconnection electric field two hours before onset.

3.3. A Detailed Examination of the Time Evolution in Each Event

[33] Figure 5 shows the detailed time series data for the 13 reconnection events from two hours before reconnection onset until two hours after. The events are denoted with numbers and times from Table 1. Two panels are shown for each event. The top panels contain the lobe magnetic field, B_L (red lines), the normal component of the magnetic field, B_Z (blue lines), and the current sheet half thickness, L (black lines). The lower panels contain the AL-index (purple lines) and the effective dayside reconnection electric field, E_D (green lines). Between the two panels, the growth phase signatures are denoted with the same letters as was used in Figures 3 and 4. Each event is centered around reconnection onset. The duration of the reconnection events are marked with grey horizontal stripes. B_Z is only shown when the spacecraft is less than one half-thickness from the current sheet center.

[34] The events can quickly be summarized as follows. Event number 1, 5 and 9 are the three events with highest E_D (green lines). They show all the classical substorm growth phase signatures with current sheet thinning (black lines), magnetic field line stretching (blue lines) and lobe pressure enhancements (red lines). After reconnection onset, there is a large decrease in the lobe pressure, and a substantial increase in the auroral electrojet (purple lines). Event number 3 and 8 occur during very low E_D. These events exhibit very little variation in B_L before and after reconnection onset. In both cases magnetic field line stretching is very low because the field lines already were relatively stretched two hours before reconnection onset. On the other hand, the current sheet thinning is very similar as in the events with strong solar wind driving. The rest of the events occur under more mixed combinations of current sheet thinning and stretching. Since it varies greatly how stretched the field lines are initially two hours before onset, the decrease in B_Z is often low.

[35] The most pronounced feature before onset is a decrease of the current sheet thickness (black lines). Current sheet thinning is seen in eight out of the eleven events where the current sheet thickness was found. These are the events 1, 3, 4, 5, 6, 8, 9 and 10. It could not be determined in the events 7 and 12, because of the rejection criteria listed in section 2.4. In the events 2 and 11 the current sheet was relatively thin the last 100 min before reconnection onset, and they are therefore not counted as thinning. These two events are instead characterized by magnetic field line stretching (blue lines) before reconnection onset. Also in event number 4 the stretching seems to dominate before reconnection onset, and thinning is only seen 60–120 min before the onset.

[36] Figure 6 shows the average current sheet half thickness for the events with thinning. The current sheet half thickness decreases from 12000 to 6000 km in 55 minutes before onset, for the eight events with thinning. This can be

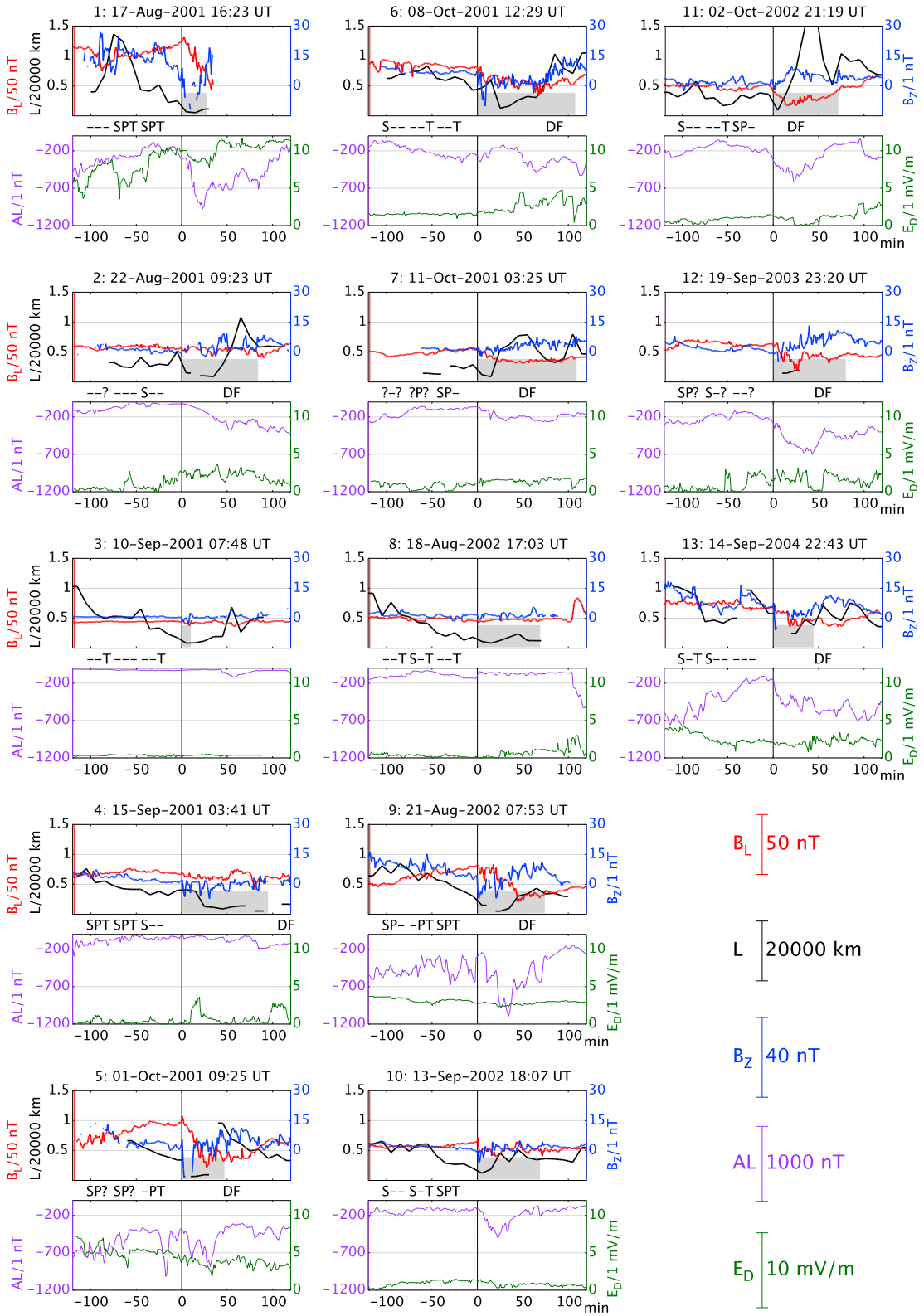

Figure 5. Time evolution of the lobe magnetic field, B_L, the current sheet half thickness, L, and the normal component of the magnetic field, B_Z (upper panels), and the AL-index and the effective dayside reconnection electric field, E_D (lower panels). B_L and L are divided by 50 nT and 20000 km respectively, to show the two variables in the same panel. For each event, the flow intervals (see Figure 4) associated with the reconnection events are marked with shaded grey stripes. Zero epoch refer to the time of reconnection onset which is shown above the upper panel of each event. The numbers refers to the events in Table 1.

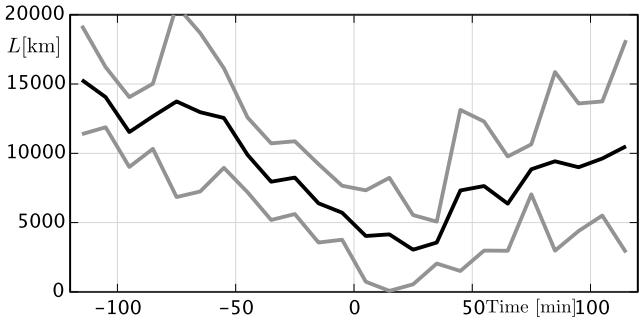

Figure 6. Average (black line) and standard deviation (gray lines) of the current sheet half thickness for those events which exhibit thinning before reconnection onset. These are the events 1, 3, 4, 5, 6, 8, 9 and 10.

compared with the average half-thickness in the reconnection region, which is 1800 ± 200 km. This estimate was done when Cluster measures the first flow reversal after reconnection onset. Note that this value would not include any micro structures of the reconnection region, because of the 10 min averaging.

3.4. Covariation Between Lobe Pressure Enhancement, Current Sheet Thinning and Field Line Stretching

[37] Increase in the lobe pressure, current sheet thinning and field line stretching can be quantified by estimating the time derivatives of B_L, L and B_Z, respectively. It is clear that the time resolution of the data would influence the value of the derivative. Figure 7 shows scatterplots of the rates of change of L, B_Z and B_L. They are calculated based on how much the variables vary during 30 min time intervals. I. e., $\Delta B_L(t) = B_L(t + 30\ \text{min}) - B_L(t)$. These plots were made to better see how the variables co-vary. Note that there are fewer points in the two lower panels than the top one, because the current sheet thickness could not always be estimated.

[38] These scatterplots reveal several features which were not clearly visible in Figure 5. Lobe pressure enhancement ($\Delta B_L > 0$) happens only during stretching ($\Delta B_Z < 0$) (top panel), and mostly during thinning ($\Delta L < 0$) (middle panel). Thinning, on the other hand, happens both for positive and negative ΔB_L. In particular, there are many samples with significant thinning centered around $\Delta B_L = 0$. Finally, thinning mainly coincides with stretching (bottom panel).

[39] Scatterplots were also examined for higher time resolutions than in Figure 7. For 10 min resolution, the points are much more uniformly distributed, and the pattern in Figure 7 is barely visible. But as the time resolution gradually decreases the pattern in Figure 7 gradually appears. This indicates that the pattern represents a real relation between the variables at the 30 min timescale, rather than a random pattern. At smaller timescales, other sources of variation may dominate the statistics.

4. Discussion

[40] The energy release during auroral substorms usually coincides with a large increase in the nightside reconnection rate. Several previous studies have addressed the relation between substorm growth phase signatures and reconnection onset. To our knowledge, all of these studies have selected events based on ground based substorm signatures. This motivated us to investigate three typical substorm growth phase signatures before nightside reconnection, identified solely from in situ measurements in the plasma sheet.

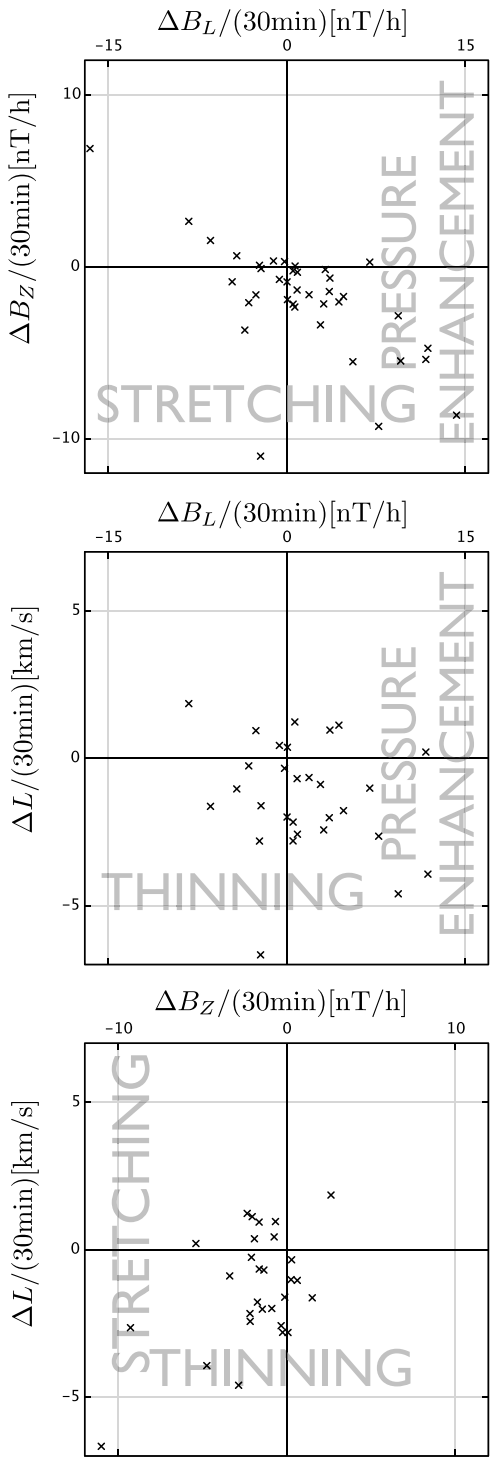

Figure 7. Covariation between magnetic field line stretching, lobe pressure enhancements and current sheet thinning, two hours before reconnection onset. These processes are quantified from the rate of change of L, B_Z and B_L between 30 min time intervals.

[41] Current sheet thinning has been observed to coincide with increase in the lobe magnetic pressure during the substorm growth phase [*McPherron et al.*, 1973; *Pulkkinen et al.*, 1991]. *Baumjohann et al.* [1992] and *Baker et al.* [1996] suggested that the increased pressure causes current sheet thinning due to the vertical pressure balance. Our results clearly show that current sheet thinning occurs whether there is lobe pressure enhancement or not. This agrees very well with the results of *Dmitrieva et al.* [2004]. The average thinning of 50% is much larger than the 20% found by *Thompson et al.* [2005] before substorm onset. In their selection criteria it was no requirement that the spacecraft should be close to the reconnection region. From this it follows that the thinning probably is nonuniform across the magnetotail.

[42] Two hours before reconnection onset we find no lobe pressure enhancement without magnetic field line stretching. This is not surprising since both processes may be signatures of an increase in the cross tail current. This indicates that the onset of near-Earth reconnection is caused by both an external and an internal factor. The external factor would be the dayside reconnection rate, which add flux to the lobes resulting in enhanced tail current and magnetic field line stretching. The stretching is needed to convert the otherwise dipolar field lines in the magnetotail, to anti-parallel field lines, which is necessary for near-Earth reconnection. This agrees with *Milan* [2009], who suggested that the magnetotail is more resistant to reconnection the more dipolar it is. No connection were found between current sheet thinning and the effective dayside reconnection electric field or with pressure enhancements in the lobes, in our study. This points to an internal mechanism as the cause for the thinning of the current sheet which brings the northern and southern lobes together before reconnection onset. The exact mechanism for current sheet thinning remains a question for further studies.

[43] The increase in the lobe magnetic field strength seen before substorm onset in studies like *Caan et al.* [1975], may lead to the hypothesis that reconnection starts when the lobe pressure reaches some critical value. Our study indicates that the change in tail configuration through thinning and stretching are more important processes for the triggering of reconnection. In many events, the lobe magnetic field is completely unchanged, or it may even decrease before the onset of reconnection. Neither is there any indication that reconnection occurs for any preferred lobe pressure. Consistent with this, *Milan et al.* [2007] found that there is no critical value of the amount of open flux which leads to reconnection. In most events there is a clear unloading signature after reconnection onset with a decrease in the lobe magnetic field magnitude. This means that magnetic flux which is added to the lobes at earlier times, is stored there until the conditions in the magnetotail is favorable for reconnection.

[44] The 50–60 min duration of the current sheet thinning found here and by *Thompson et al.* [2005], is quite in line with the observed delay between the dayside energy input and nightside energy release. *Bargatze et al.* [1985] found that the westward electrojet shows one response to changes in the solar wind energy input after 15–30 min, and another response after 55–70 min. Likewise, *Eriksson et al.* [2000] found a peak in the cross-correlation function between the dayside reconnection electric field and the polar cap flux transport at 55 min. In both studies, these lags were interpreted to be due to the release of stored magnetic energy in the lobes. This gives further evidence that the thinning influences when the unloading takes place.

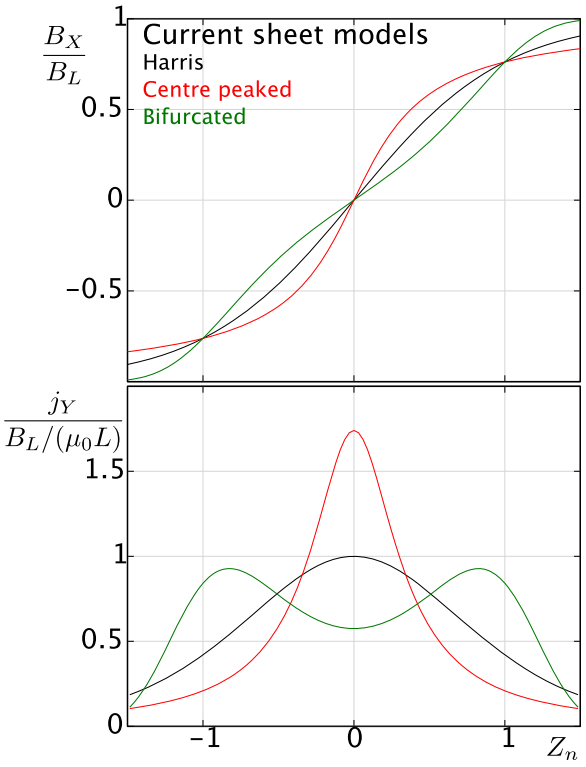

Figure A1. The magnetic field B_X and current density j_Y, as a function of the distance from the current sheet center, for three different current distributions. The variables are normalized with the lobe magnetic field B_L, and the current sheet half thickness L, corresponding to $B_X(Z = L) = 0.76B_L$.

[45] The reconnection events were identified solely from in situ measurements in the plasma sheet [*Østgaard et al.*, 2009]. To address the role of these local events in the large scale tail dynamics, the timing of the reconnection onset was compared with other measurements from the ionosphere and the magnetotail in Figure 4. It was found that most events follow the typical substorm time sequence with tailward flow followed by earthward flow and dipolarization. This is consistent with an X-line forming somewhere earthward of the spacecraft and then moving tailward. This makes the events somewhat unusual since reconnection events usually are observed tailward of the Cluster apogee [*Nagai et al.*, 2005]. However, [*Miyashita et al.*, 2009] have found indications that the reconnection region initially forms at a distance of X = −16 to −20 R_E, on average.

[46] *Milan et al.* [2007] found the average duration of nightside reconnection events to be 72 min from global imaging. Our enhanced flow periods last 10–109 min with an average of 72 min. The exact durations would depend on how the flow intervals are defined, but by inspecting Figure 4 it is clear that the reconnection onsets usually causes an enhanced plasma flow for about an hour. This agrees well with the duration of the flows given by *Baumjohann et al.* [2000], but is 3–4 times longer than the

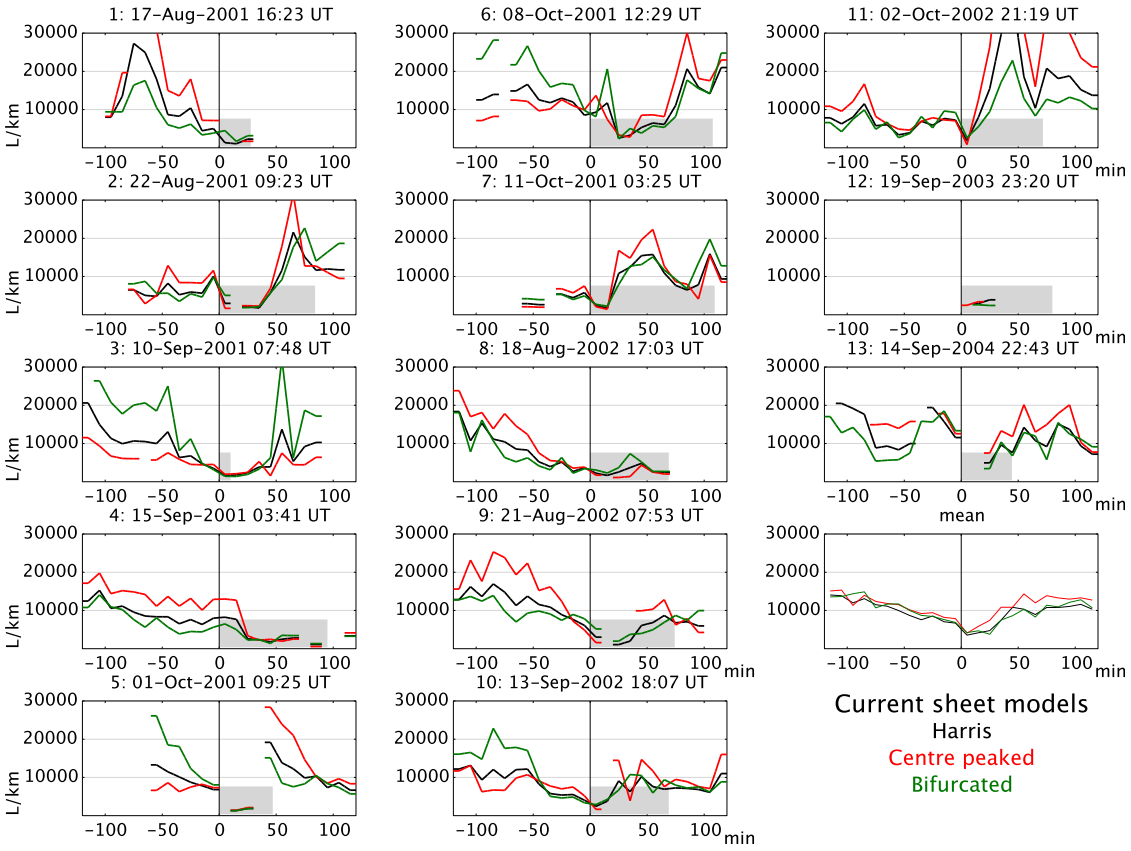

Figure A2. The current sheet half thickness L, for the three current sheet models in Figure A1 in the same format as Figure 5.

average duration of a bursty bulk flow (BBF) [*Angelopoulos et al.*, 1994; *Cao et al.*, 2006]. This could mean that BBFs last shorter the further from the reconnection region they are observed.

[47] Substorm onset in the ionosphere can be identified from auroral images [e.g., *Frey et al.*, 2004] and from increase in the auroral electrojet [e.g., *Tanskanen et al.*, 2005]. From the summary plot (Figure 4) it is clear that the reconnection events are associated with both types. In the six events with auroral images there is either a substorm onset or an auroral intensification close to the events. But the reconnection onsets identified from in situ measurements can occur both before and after the auroral substorm onsets. This is consistent with that reconnection alone is not sufficient for substorms to occur. Although the AE index is too inaccurate for detailed study of the substorm development in single events, it is no doubt that there usually is an increase in the electrojet after reconnection onset. It is interesting to note that the two events (3 and 8) with most stable lobe magnetic field, also are those with weakest signature in AL. Also at midlatitudes, the magnetic signatures during substorm expansion onset is known to be correlated with the pressure variations in the magnetotail, as shown by *Yamaguchi et al.* [2004].

5. Conclusions

[48] Reconnection in the magnetotail is not dependent on a period of increase in the lobe magnetic field strength the last hour before onset. Neither is there any preferred value of the lobe magnetic field which seems to trigger reconnection. Current sheet thinning seems to be a more important precondition for reconnection onset than the increase of the lobe pressure. The average current sheet thickness decreases from 24000 to 12000 km in about 55 min before reconnection onset. No correlation between the solar wind driving and the current sheet thinning was found. This points to an internal mechanism for current sheet thinning. A challenge for future studies could be to determine this mechanism.

Appendix A: Different Cross Tail Current Distributions

[49] The current sheet model determines how the magnetic field measurements are transformed into Z-positions in the current sheet. Different models would give different results, and applying a wrong model might cause the estimated current sheet thickness to vary when Cluster crosses the current sheet, even if the real thickness is constant. In this section, we investigate the effect different models has on the estimation of the thickness, and we try to determine whether our conclusions about current sheet thinning hold, if the current sheet distribution is different from a Harris current sheet.

[50] Two models have been compared with the Harris current sheet model. One is center-peaked and the other one is bifurcated. The difference between the models is the

transformation of the magnetic field in equation (2). For the center-peaked, it is given as

$$Z_n = 0.299 \sinh\left(1.92 \tanh^{-1}\frac{B_{Xi}}{B_L}\right), \quad \text{(A1)}$$

while it is

$$Z_n = 0.521 \sinh^{-1}\left(3.34 \tanh^{-1}\frac{B_{Xi}}{B_L}\right), \quad \text{(A2)}$$

for the bifurcated model. The magnetic field and current density as a function of Z_n, are shown in Figure A1. Both models have been adjusted such that $B_X(Z = \pm L))$ is the same as in the Harris sheet model, namely 76% of the lobe magnetic field. It must be emphasized that the two models are not derived from any physical considerations, and were only chosen because of their ability to reproduce the desired patterns.

[51] The estimated half thicknesses of the current sheet for the different models are shown in Figure A2 in the same format as in Figure 5. It is immediately clear that the estimated thickness can vary considerably between the models, but that they usually follow a similar time evolution. The differences between the models mostly cancel out in the average in the bottom panel. The main conclusions which were drawn about current sheet thinning earlier in this paper, seem to hold. In those events where the three models give similar time evolution, the current sheet is thinning before reconnection onset. These are event numbers 1, 3, 4, 8, 9 and 10. It is relatively thin the last hour before onset in event numbers 2, 7 and 11. Event numbers 5 and 6 are uncertain because the three models give different time evolutions.

[52] **Acknowledgments.** We acknowledge the Cluster CIS PI Iannis Dandouras, the Cluster FGM PI Elizabeth Lucek, and the use of NASA/GSFC's Space Physics Data Facility's OMNIWeb service and OMNI data. Work at FMI was funded by Academy of Finland projects 108518 and 128632.

[53] Masaki Fujimoto thanks the reviewers for their assistance in evaluating this paper.

References

Angelopoulos, V., C. F. Kennel, F. V. Coroniti, R. Pellat, M. G. Kivelson, R. J. Walker, C. T. Russell, W. Baumjohann, W. C. Feldman, and J. T. Gosling (1994), Statistical characteristics of bursty bulk flow events, *J. Geophys. Res.*, *99*(A11), 21,257–21,280, doi:10.1029/94JA01263.

Asano, Y., R. Nakamura, W. Baumjohann, A. Runov, Z. Vörös, M. Volwerk, T. L. Zhang, A. Balogh, B. Klecker, and H. Réme (2005), How typical are atypical current sheets?, *Geophys. Res. Lett.*, *32*, L03108, doi:10.1029/2004GL021834.

Baker, D. N., T. I. Pulkkinen, V. Angelopoulos, W. Baumjohann, and R. L. McPherron (1996), Neutral line model of substorms: Past results and present view, *J. Geophys. Res.*, *101*(A6), 12,975–13,010, doi:10.1029/95JA03753.

Balogh, A., et al. (2001), The cluster magnetic field investigation: Overview of in-flight performance and initial results, *Ann. Geophys.*, *19*(10–12), 1207–1217, doi:10.5194/angeo-19–1207–2001.

Bargatze, L. F., D. N. Baker, R. L. McPherron, and E. W. Hones Jr. (1985), Magnetospheric impulse response for many levels of geomagnetic activity, *J. Geophys. Res.*, *90*(A7), 6387–6394.

Baumjohann, W., G. Paschmann, N. Sckopke, C. A. Cattell, and C. W. Carlson (1988), Average ion moments in the plasma sheet boundary layer, *J. Geophys. Res.*, *93*(A10), 11,507–11,520.

Baumjohann, W., G. Paschmann, and C. A. Cattell (1989), Average plasma properties in the central plasma sheet, *J. Geophys. Res.*, *94*(A6), 6597–6606.

Baumjohann, W., G. Paschmann, and H. Luhr (1990), Pressure balance between lobe and plasma sheet, *Geophys. Res. Lett.*, *17*(1), 45–48.

Baumjohann, W., G. Paschmann, and T. Nagai (1992), Thinning and expansion of the substorm plasma sheet, *J. Geophys. Res.*, *97*(A11), 17,173–17,175, doi:10.1029/92JA01519.

Baumjohann, W., T. Nagai, A. Petrukovich, T. Mukai, T. Yamamoto, and S. Kokubun (2000), Substorm signatures between 10 and 30 Earth radii, in *Coordinated Measurements of Magnetospheric Processes (Advances in Space Research)*, vol. 25, edited by C. T. Russell, pp. 1663–1666, Pergamon, Oxford, U. K.

Birn, J. (1987), Magnetotail equilibrium theory: The general three-dimensional solution, *J. Geophys. Res.*, *92*(A10), 11,101–11,108.

Borg, A. L., et al. (2007), Simultaneous observations of magnetotail reconnection and bright X-ray aurora on 2 October 2002, *J. Geophys. Res.*, *112*, A06215, doi:10.1029/2006JA011913.

Caan, M. N., R. L. McPherron, and C. T. Russel (1975), Substorms and interplanetary magnetic field effects on the geomagnetic tail lobes, *J. Geophys. Res.*, *80*(1), 191–194.

Cao, J. B., et al. (2006), Joint observations by Cluster satellites of bursty bulk flows in the magnetotail, *J. Geophys. Res.*, *111*, A04206, doi:10.1029/2005JA011322.

Dmitrieva, N. P., V. A. Sergeev, and M. A. Shukhtina (2004), Average characteristics of the midtail plasma sheet in different dynamic regimes of the magnetosphere, *Ann. Geophys.*, *22*(6), 2107–2113, doi:10.5194/angeo-22–2107–2004.

Eriksson, S., R. E. Ergun, C. W. Carlson, and W. Peria (2000), The cross-polar potential drop and its correlation to the solar wind, *J. Geophys. Res.*, *105*(A8), 18,639–18,653, doi:10.1029/2000JA900033.

Fairfield, D. H. (1985), Solar wind control of magnetospheric pressure (CDAW 6), *J. Geophys. Res.*, *90*(A2), 1201–1204.

Frey, H., S. Mende, V. Angelopoulos, and E. Donovan (2004), Substorm onset observations by IMAGE-FUV, *J. Geophys. Res.*, *109*, A10304, doi:10.1029/2004JA010607.

Harris, E. G. (1962), On a plasma sheath separating regions of oppositely directed magnetic field, *Nuovo Cimento*, *23*, 115–121.

Hones, E. W., Jr. (Ed.) (1984), Plasma sheet behavior during substorms, in *Magnetic Reconnection in Space and Laboratory Plasmas*, *Geophys. Monogr. Ser.*, vol. 30, pp. 178–184, AGU, Washington, D. C.

Kan, J. R., and L. C. Lee (1979), Energy coupling function and solar wind-magnetosphere dynamo, *Geophys. Res. Lett.*, *6*(7), 577–580.

Kaymaz, Z., G. L. Siscoe, N. A. Tsyganenko, and R. P. Lepping (1994), Magnetotail views at 33 R_E: IMP 8 magnetometer observations, *J. Geophys. Res.*, *99*(A5), 8705–8730, doi:10.1029/93JA03564.

Khrabrov, A. V., and B. U. Ö. Sonnerup (1998), Error estimates for minimum variance analysis, *J. Geophys. Res.*, *103*(A4), 6641–6651, doi:10.1029/97JA03731.

King, J., and N. Papitashvili (2005), Solar wind spatial scales in and comparisons of hourly Wind and ACE plasma and magnetic field data, *J. Geophys. Res.*, *110*, A02104, doi:10.1029/2004JA010649.

McPherron, R. L., C. T. Russel, and M. P. Aubry (1973), Satellite studies of magnetospheric substorms on August 15, 1968: 9. Phenomenological model for substorms, *J. Geophys. Res.*, *78*(16), 3131–3149.

Milan, S. E. (2009), Both solar wind-magnetosphere coupling and ring current intensity control of the size of the auroral oval, *Geophys. Res. Lett.*, *36*, L18101, doi:10.1029/2009GL039997.

Milan, S. E., A. Grocott, C. Forsyth, S. M. Imber, P. D. Boakes, and B. Hubert (2009), A superposed epoch analysis of auroral evolution during substorm growth, onset and recovery: Open magnetic flux control of substorm intensity, *Ann. Geophys.*, *27*(2), 659–668, doi:10.5194/angeo-27–659–2009.

Milan, S. E., G. Provan, and B. Hubert (2007), Magnetic flux transport in the Dungey cycle: A survey of dayside and nightside reconnection rates, *J. Geophys. Res.*, *112*, A01209, doi:10.1029/2006JA011642.

Milan, S. E., P. D. Boakes, and B. Hubert (2008), Response of the expanding/contracting polar cap to weak and strong solar wind driving: Implications for substorm onset, *J. Geophys. Res.*, *113*, A09215, doi:10.1029/2008JA013340.

Miyashita, Y., et al. (2009), A state-of-the-art picture of substorm-associated evolution of the near-Earth magnetotail obtained from superposed epoch analysis, *J. Geophys. Res.*, *114*, A01211, doi:10.1029/2008JA013225.

Nagai, T., M. Fujimoto, R. Nakamura, W. Baumjohann, A. Ieda, I. Shinohara, S. Machida, Y. Saito, and T. Mukai (2005), Solar wind control of the radial distance of the magnetic reconnection site in the magnetotail, *J. Geophys. Res.*, *110*, A09208, doi:10.1029/2005JA011207.

Nakamura, R., et al. (1999), Response of the midtail electric field to enhanced solar wind energy input, *J. Geophys. Res.*, *104*(A8), 17,299–17,310, doi:10.1029/1999JA900166.

Nakamura, R., et al. (2002a), Fast flow during current sheet thinning, *Geophys. Res. Lett.*, *29*(23), 2140, doi:10.1029/2002GL016200.

Nakamura, R., et al. (2002b), Motion of the dipolarization front during a flow burst event observed by Cluster, *Geophys. Res. Lett.*, *29*(20), 1942, doi:10.1029/2002GL015763.

Østgaard, N., K. Snekvik, A. L. Borg, A. Åsnes, A. Pedersen, M. Øieroset, T. Phan, and S. E. Haaland (2009), Can magnetotail reconnection produce the auroral intensities observed in the conjugate ionosphere?, *J. Geophys. Res.*, *114*, A06204, doi:10.1029/2009JA014185.

Pulkkinen, T. I., D. N. Baker, D. H. Fairfield, R. J. Pellinen, J. S. Murphree, R. D. Elphinstone, R. L. McPherron, J. F. Fennell, R. E. Lopez, and T. Nagai (1991), Modeling the growth phase of a substorm using the tsyganenko model and multi-spacecraft observations: CDAW-9, *Geophys. Res. Lett.*, *18*(11), 1963–1966, doi:10.1029/91GL02002.

Rème, H., et al. (2001), First multispacecraft ion measurements in and near the earth's magnetosphere with the identical cluster ion spectrometry (CIS) experiment, *Ann. Geophys.*, *19*(10–12), 1303–1354, doi:10.5194/angeo-19–1303–2001.

Runov, A., et al. (2006), Local structure of the magnetotail current sheet: 2001 Cluster observations, *Ann. Geophys.*, *24*(1), 247–262, doi:10.5194/angeo-24–247–2006.

Sharma, A. S., et al. (2008), Transient and localized processes in the magnetotail: A review, *Ann. Geophys.*, *26*(4), 955–1006, doi:10.5194/angeo-26–955–2008.

Shukhtina, M., N. Dmitrieva, N. Popova, V. Sergeev, A. Yahnin, and I. Despirak (2005), Observational evidence of the loading-unloading substorm scheme, *Geophys. Res. Lett.*, *32*, L17107, doi:10.1029/2005GL023779.

Sonnerup, B. U. Ö. (1979), Magnetic field reconnection, in *Solar System Plasma Physics*, edited by L. J. Lanzerotti, C. F. Kennel, and E. N. Parker, p. 46, North Holland Publ., Amsterdam.

Tanskanen, E. I., J. A. Slavin, A. J. Tanskanen, A. Viljanen, T. I. Pulkkinen, H. E. J. Koskinen, A. Pulkkinen, and J. Eastwood (2005), Magnetospheric substorms are strongly modulated by interplanetary high-speed streams, *Geophys. Res. Lett.*, *32*, L16104, doi:10.1029/2005GL023318.

Thompson, S., M. Kivelson, K. Khurana, R. McPherron, J. Weygand, A. Balogh, H. Reme, and L. Kistler (2005), Dynamic Harris current sheet thickness from Cluster current density and plasma measurements, *J. Geophys. Res.*, *110*, A02212, doi:10.1029/2004JA010714.

Yamaguchi, R., H. Kawano, S. Ohtani, S. Kokubun, and K. Yumoto (2004), Total pressure variations in the magnetotail as a function of the position and the substorm magnitude, *J. Geophys. Res.*, *109*, A03206, doi:10.1029/2003JA010196.

A. L. Borg, European Space Research and Technology Center, European Space Agency, Postbus 299, NL-2200 Noordwijk, Netherlands. (anette.l.borg@gmail.com)

E. I. Gordeev, Department of Physics of Earth, Saint Petersburg State University, 1A Ulyanovskaya St., Petrodvoretz, 198504 St. Petersburg, Russia. (evgeniy_gordeev@yahoo.com)

L. Juusola, K. Snekvik, and E. Tanskanen, Finnish Meteorological Institute, PO Box 503, FI-00101 Helsinki, Finland. (kristian.snekvik@fmi.fi; eija.tanskanen@fmi.fi)

K. M. Laundal, Teknova AS, Gimlemoen 19, N-4639 Kristiansand, Norway. (kalle.laundal@gmail.com)

N. Østgaard, Department of Physics and Technology, University of Bergen, PO Box 7803, N-5020 Bergen, Norway. (nfyno@ift.uib.no)